RESEARCH ARTICLE

ADVANCED
MATERIALS
INTERFACES
Open Access

www.advmatinterfaces.de

Sprayable Thermoset Nanocomposite Coatings Based on Silanized-PEG/ZnO to Prevent Microbial Infections of Titanium Implants

Davide Morselli,* Ramona Iseppi, Evie L. Papadopoulou, Giovanni Bolelli, Carla Sabia, Micaela Degli Esposti,* and Paola Fabbri

Post-surgery microbial infections are still one of the main reasons for implant failure, which results in very high physical and psychological pain for the patient and an increased cost for the healthcare system. A polymer nanocomposite antibacterial coating on titanium implants represents a valuable alternative to the more expensive and energy-consuming technological solutions nowadays used. In this regard, a sprayable thermoset nanocomposite composed of silanized-terminals polyethylene glycol (PEG)/ZnO nanoparticle is herein proposed. Initially, PEG's terminals' solvent-free silanization and curing are studied by Fourier Transform Infrared and μRaman spectroscopies. Scanning Electron Microscope investigations and scratch tests have shown that the spraying procedure optimization and the oxidation treatment of the titanium substrate lead to a homogeneous coverage and improved adhesion of the coatings. The antibacterial activity is tested against not only both *S. aureus* and *P. aeruginosa* bacterial American Type Culture Collection strains, but also using very aggressive antibiotic-resistant clinical strains. Interestingly, antibacterial activity, evaluated by time-killing tests, is observed for all tested bacterial strains. Live/dead tests further confirm that 5 wt% of ZnO allows obtaining a bacteriostatic activity within 24 h, whereas a complete growth inhibition (bactericidal activity) of both tested strains is observed for coatings with 20 wt% of ZnO nanoparticles.

1. Introduction

The aging of the world population[1] has been leading to an overall increase in medical treatments and healthcare costs.[2,3] In particular, orthopedic and dental surgeries using artificial titanium implants have become frequent operations with millions of people treated every year.[4,5] Although titanium implants are characterized by suitable mechanical and chemical properties, corrosion resistance, and biocompatibility, microbial infections are still one of the main reasons for implant failure.[6–8] Despite the improvements in the healthcare quality in the last two decades, the probability of infection during an orthopedic surgical procedure is still in the range of 2–5%.[9] This range might seem a rather low value, however, different aspects should be considered for a fair evaluation. When failure is due to implant infection, the most common solution is to remove the infected implanted part by a second surgery and a massive treatment of the patient with

D. Morselli, M. Degli Esposti, P. Fabbri
Department of Civil, Chemical
Environmental and Materials Engineering (DICAM)
Università di Bologna
Via Terracini 28, Bologna 40131, Italy
E-mail: davide.morselli6@unibo.it; micaela.degliesposti@unibo.it

D. Morselli, M. Degli Esposti, P. Fabbri
National Interuniversity Consortium of Materials Science
and Technology (INSTM)
Via Giusti 9, Firenze 50121, Italy

R. Iseppi, C. Sabia
Department of Life Sciences
Università di Modena e Reggio Emilia
Via Campi 103/287, Modena 41125, Italy

E. L. Papadopoulou
Smart Materials Group
Istituto Italiano di Tecnologia
Via Morego 30, Genova 16163, Italy

G. Bolelli
Department of Engineering "Enzo Ferrari"
Università di Modena e Reggio Emilia
Via Vivarelli 10/1, Modena 41125, Italy

antibiotics. This procedure is then followed, after an appropriate amount of time, by a third surgery to introduce the new implant. For the unlucky patient, this long, painful, and annoying process is an experience of extreme suffering from both a physical and psychological point of view. Furthermore, this represents an enormous expense for the healthcare system if compared to a regular single-operation procedure, which typically involves a short stay in the hospital. Therefore, antibacterial activity is an important feature for titanium implants, preventing the development of post-surgery microbial infections and reducing the chance of the aforementioned severe complications. The infections associated with medical devices can progress rapidly as planktonic bacteria adhere to the implant interface and eventually evolve into biofilm.[10] Biofilm is defined as a structured community of microorganisms, enclosed in a self-produced polymeric matrix, adhering to an inert or living surface in an aqueous medium. Biofilms are very heterogeneous communities characterized by multiple interactions between the different microbial species that constitute them,[11] allowing microbial cells to continuously adapt to extreme conditions. Biofilms can form on biotic and abiotic surfaces, such as solid surfaces of medical devices, epithelia, mucous membranes, and dental plaques. A fundamental biological characteristic of the biofilm is the presence of a self-produced extracellular matrix (EPS, Extracellular Polymeric Substance), composed of a mix of polysaccharides, water, ions, DNA, and proteins released by the biofilm bacteria,[12] which behaves as a barrier for external agents (e.g., disinfectants and antimicrobials).

In the last decade, several approaches have been proposed to develop antibacterial titanium implants.[13,14] Among them, the surface modification with an active material is indeed the most promising method, which allows to envision a straightforward technology transfer from lab to industry.[14,15]

The modification of the titanium implant surface with an antibacterial agent, such as ZnO, CeO_2, TiO_2, or Ag nanoparticles (NPs), is an extensively explored option.[16,17] In particular, metal oxides are most interesting from an industrial point of view because of their average cost, which is lower with respect to Ag NPs. Typically, the antimicrobial properties of inorganic oxides have to be triggered by UV light irradiation, which induces the formation of the so-called Reactive Oxygen Species (ROSs) and thus the desired antibacterial activity.[18] Interestingly, Prasanna and Vijayaraghavan[19] have shown that ZnO can induce ROSs formation even in the dark. Furthermore, they have shown that antibacterial activity in the dark is mainly attributed to ROSs originating through the interaction of water/moisture with superoxide species.[19] More in detail, Xu et al. have demonstrated that the formation of ROSs can be catalyzed in the oxygen vacancies on the surface of ZnO particles when are surrounded by an aqueous environment.[20] This specific property of ZnO has been further exploited to obtain antibacterial activity in PMMA-based composite fibers with potential application in the biomedical field.[21]

The main drawbacks of the direct modification of the implant surface with NPs are associated with the release of NPs within the patient's body and the high production cost to apply this kind of inorganic coating. This is due to the large number of NPs and the high energy consumption of the technologies needed to fully cover the implant surface.[15] It is known that the antibacterial properties are not enhanced linearly over a given amount of NPs,[22] which depends on the material morphology and nature. Therefore, a further increase in the NPs content only results in an overall increase in the final production costs with no further benefit in terms of antibacterial performance.
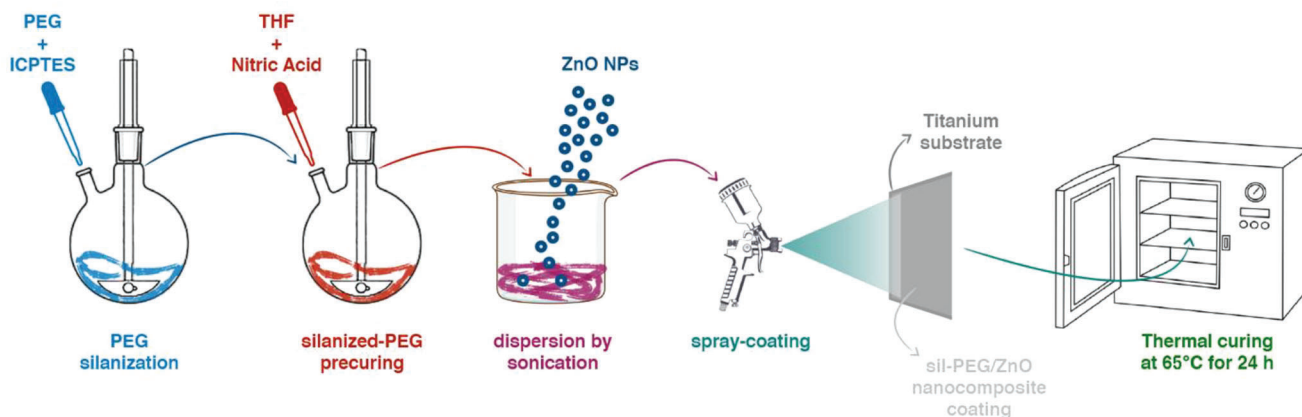
A possible solution to the aformentioned drawbacks is found in coating the titanium implant surface with a polymer/NPs composite material.[23] The use of polymer/NPs composites allows to use less energy-consuming particle deposition methods and a lower amount of NPs with respect to the conventional technologies used for full-ceramic coatings.[20,22] A further advantage of using NPs embedded in a polymeric cross-linked network is to limit the NPs release and mineralization with the consequent release of high concentrations of metallic ions. Indeed, this approach requires a polymeric matrix that has to be biocompatible and insoluble in water-based media since the application is envisioned in body fluids. Polyethylene glycol (PEG) and PEG-derived materials have been widely proposed in various biomedical applications thanks to their known biocompatibility and relatively low cost.[24–26] In addition, PEG can be easily spray-coated and it is characterized by antifouling properties, which can significantly reduce bacteria adhesion.[27]

The combination of PEG and ZnO NPs can lead to a suitable composite material for preparing a sprayable antibacterial coating for titanium implants. However, a thermoset polymer that can form a cross-linked macromolecular network, which ensures the stability of the coating and improves adhesion to the metallic substrate, is the most appropriate for this application. By exploiting and adjusting the first step of the procedure typically reported to produce SiO_2/polymer hybrids,[28,29] it is possible to obtain a PEG-based thermoset formulation suitable for coating application. In particular, using 3-isocyanatopropyltriethoxysilane (ICPTES), the hydroxyl terminal groups of the polymer can be silanized[30] thus obtaining a silane-terminated PEG (sil-PEG), which can be thermally cured similarly to a thermoset resin. This would allow to obtain the desired material, which could be sprayable, thermal-curable, and thus insoluble in water and eventually antibacterial even in dark conditions through the addition of the selected NPs.

The scope of this study is to develop a nanocomposite combining ZnO NPs and a PEG-derived curable resin to obtain sprayable antibacterial coatings to prevent bacterial infections on titanium implants. Specifically, we initially optimize the functionalization of PEG and the spray-coating and curing procedures used to obtain homogeneous transparent coatings. After the characterization of their morphological aspects and scratch resistance, the prepared coatings have been extensively studied on different bacterial strains deriving from both ATCC collections and real infected titanium prostheses, in order to explore the suitability and reliability of the proposed composite material and coating method, as a potential alternative to the currently used bare inorganic materials.

2. Results and Discussion

In brief, the formulations for spray-coating have been prepared following **Scheme 1**. PEG has been initially functionalized and consequently diluted in tetrahydrofuran (THF), where ZnO NPs (<100 nm) have then been added as antibacterial agents in different ratios (1, 5, 10, and 20 wt%). The so-obtained suspensions

2300178 (2 of 13)

**ADVANCED
SCIENCE NEWS**

www.advancedsciencenews.com

**ADVANCED
MATERIALS
INTERFACES**
Open Access

www.advmatinterfaces.de

Scheme 1. Schematization of the whole process to produce the nanostructured composite coatings.

have been then sprayed onto titanium substrates and cured at 65 °C for 24 h (more experimental details in Section 4). This procedure allows to achieve a homogeneous nanocomposite coating (≈ 10 µm thick) that does not significantly alter the aspect of the used titanium substrate (Figure S1, Supporting Information).

More in detail, the hydroxyl terminals of PEG have been replaced with ethoxy silane groups by a solvent-free reaction with 3-isocyanatopropyltriethoxysilane (ICPTES) (more experimental details in Section 4) resulting in the formation of triethoxysilane-terminated PEG (sil-PEG), as summarized in the silanization reaction reported in **Scheme 2**.
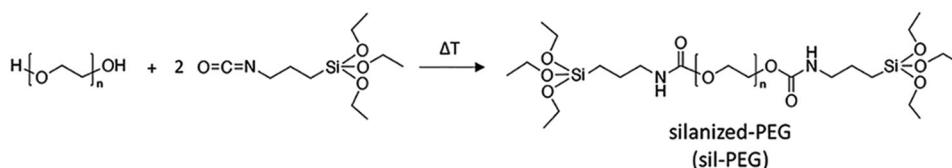
The functionalization reaction has been followed by Fourier Transform Infrared (FT-IR) spectroscopy, monitoring the variation of the peak at 2270 cm^{-1}, which is associated with the stretching of the isocyanate group.[31] As shown in **Figure 1**A and highlighted in Figure 1B, the intensity of the peak associated with the isocyanate group (2270 cm^{-1}) decreases with time, indicating that ICPTES is reacting. The increase of the peak at ≈ 1720 cm^{-1}, assigned to the bending of the urethane carbonyl group (O=C—N—H),[32] is also showing that the reaction is taking place as desired (Figure 1A,B). The intensity of this peak increases simultaneously with the decrease of the peak at 2270 cm^{-1}, indicating that the silanization process can be considered finalized after ≈ 90 min. In detail, the intensity of the peak at 2270 cm^{-1} has been normalized (as described in Experimental Section) and the conversion (X) of the isocyanate group has been calculated by Equation 1 and plotted as a function of the reaction time (Figure 1C). The data have been then fitted (Figure 1C), providing deeper insight into the reaction kinetics and the reaction order. In particular, it has been observed that the kinetic curve can be divided into three stages: in the initial 30 min, the reaction rate is very high, then it becomes slower in the range of 30–90 min

and after 90 min no further significant variation of the peak can be observed.

The as-obtained triethoxysilane terminals of sil-PEG (in solution of THF) have been substituted by hydroxyl groups using nitric acid as a catalyst as reported in **Scheme 3** (pre-curing step). Afterward, the curing step allows cross-linking of the newly formed hydroxy silane-terminated PEG (sil-PEG-OH) at low temperature (65 °C), leading to the formation of Si—O—Si cross-links among the oligomeric monomers and water as the only by-product (Scheme 3, more details in Section 4).

The formation of a cross-linked polymeric network can also be observed by FT-IR analysis. It can be noticed that after the curing process, from the background of the FT-IR spectrum of neat PEG, presented in **Figure 2**A, appears a low-intensity peak centered at ≈ 800 cm^{-1} that is assigned to the symmetric stretching mode of the Si—O—Si bond.[33]

The curing of the polymer can be further confirmed by Raman spectroscopy. In Figure 2B, the comparison of the normalized Raman spectra of the uncured and the cured polymer is depicted. In the spectrum of the uncured sample, in addition to all the characteristic peaks of PEG,[34] a small peak at 658 cm^{-1} is seen, attributed to the symmetrical Si(OR)$_3$ stretching[35–37] of the triethoxysilanes, which disappears after curing. The intensity of the 584 cm^{-1} band (due to silanol vibrations) is decreased post-curing due to the cross-linking of the siloxane network.[36] In addition, after curing there is an increase in the intensity of two peaks at 846 and 1130 cm^{-1}, which are typically attributed to C—O stretching and CH$_2$ rocking of PEG. The fact that the intensity of these peaks increases after curing can be also attributed to the formation of Si—O—Si bonds as previously observed.[37,38] Finally, the appearance of three new weak shoulders after curing at 813, 893, and 1030 cm^{-1}, can be considered a further confirmation of the

Scheme 2. Reaction scheme of the silanization process.

**ADVANCED
SCIENCE NEWS**

www.advancedsciencenews.com

**ADVANCED
MATERIALS
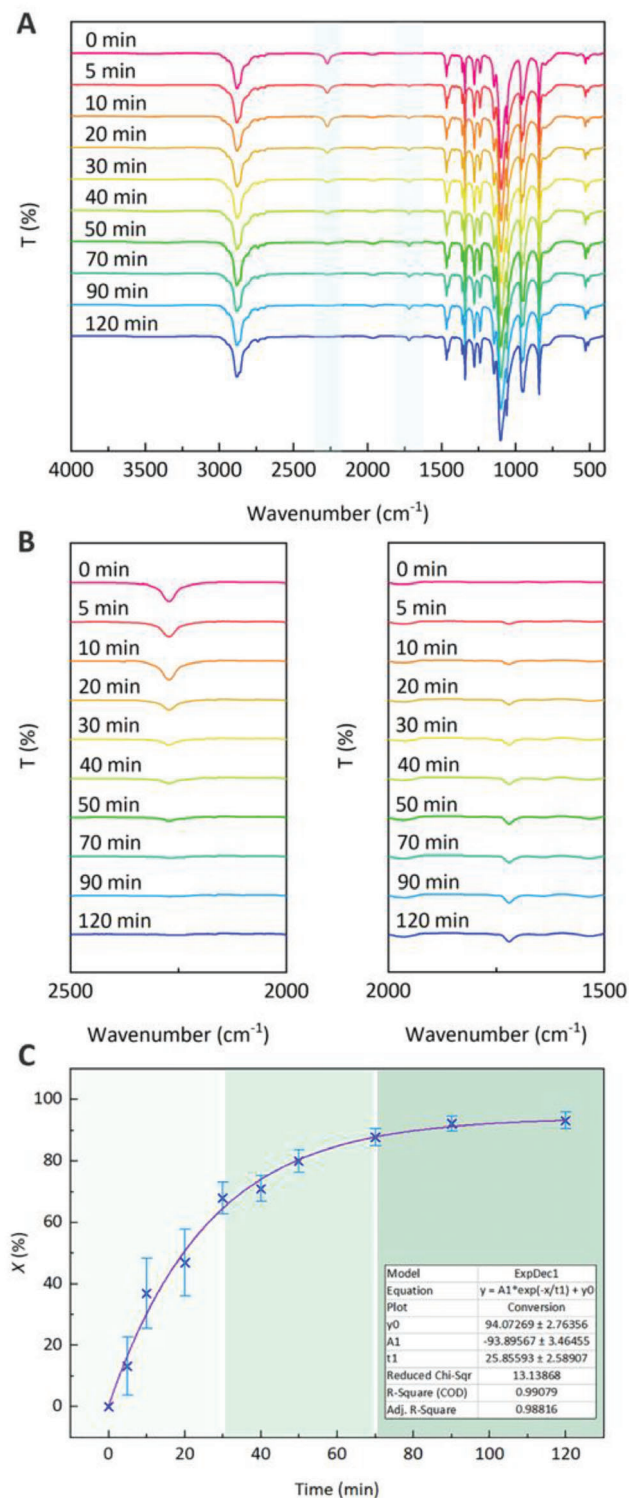INTERFACES**

www.advmatinterfaces.de

Figure 1. A) FT-IR spectra of the silanization reaction mixture at different time intervals. B) Magnification of the spectral areas highlighted in light blue in Figure 1A. C) Kinetics of the silanization reaction shown as ICPTES conversion (*X*, calculated by Equation 1) as a function of the time.

siloxane cross-link formation. These three peaks are typically attributed to SiO_4 stretching, which is structurally very similar to what is formed as a cross-linking bond between PEG chains.[39,40]

The development of a covalently bonded macromolecular network is also supported by the extractable fraction (f) calculated by Equation 2 (experimental details reported in Section 4). Figure 2C clearly shows a very low extracted fraction of ≈ 2 wt% for the cured sil-PEG sample, indicating that the formation of a covalent 3D network is achieved. Moreover, the introduction of the ZnO NPs does not significantly affect the formation of the polymeric cross-linked network showing, for the composite samples, f values in the range between 1 and 2.5 wt% that are comparable with the cured neat sil-PEG (Figure 2C).

The morphology of the coatings and homogeneity of the NPs dispersion have been investigated by a Scanning Electron Microscope equipped with a Field Emission source (FESEM). As shown by back-scattered electron images presented in **Figure 3**, the neat sil-PEG coating presents a smooth surface that homogeneously covers the titanium substrate. The composite coatings are characterized by exposed NPs that are quite homogeneously distributed, but not very highly dispersed. In particular, it is possible to observe that some small aggregates of a few micrometers are present in all NP-containing samples. However, the NPs do not alter the homogeneity of the coating which does not present significant defects.

The adhesion of the composite coating is significantly compromised when titanium surface oxidation is not carried out. More in detail, scratch tests revealed that the increment of the NPs content reduces the coatings' adhesion (Figure S2A, Supporting Information), although the cross-linking density of the coating is not affected (Figure 2C). In fact, up to a maximum load of 30 N, the neat sample did not delaminate (Figure S2B,C, Supporting Information): the indenter only exerted a plowing and wedging action, plastically displacing the cross-linked sil-PEG to the sides and the front of the scratch track (Figure S2C, Supporting Information). This testifies to a ductile/strong mechanical response according to the categorization by Jiang and co-workers.[41] By contrast, NP-containing coatings delaminated at progressively lower loads. Even with as low as 1 wt% NPs, failure occurred at ≈ 5 N (Figure S2A, Supporting Information). With 5 wt% NPs or more, the coating delaminated at the very beginning of the test (Figure S2C, Supporting Information). This shows the poor adhesion of the NP-reinforced polymer to the untreated Ti surface. Moreover, the NP-containing coatings do not flow as homogeneously as the neat polymer to the sides of the indenter (Figure S2C, Supporting Information). The irregularity of the plastic flow suggests that the NPs compromise the ductility of the coating, which is consistent with the embrittlement effect reported by Kurcku et al. for polymer matrices loaded with hard particles.[42]

On the other hand, when coatings are deposited onto oxidized Ti substrates, no large-scale failure (e.g., delamination) is observed up to the highest NPs content used in this work (**Figure 4**A), indicating a significantly enhanced adhesion. Magnified views (Figure 4B) only show minor damage, whose morphology changes with the addition of nanoparticles. Specifically, the neat coating exhibits ductile tearing, like the one
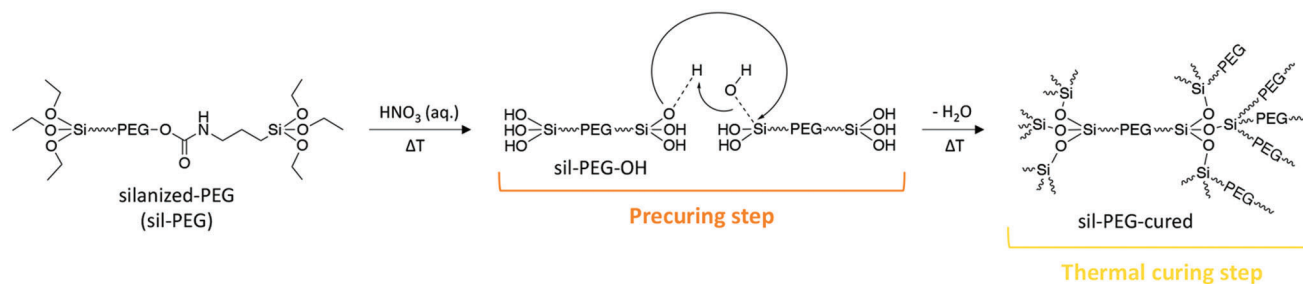
Scheme 3. Reaction scheme of the pre-curing and curing processes.

observed elsewhere.[41] The morphology of those tears also resembles the typical damage produced when a blunt, hard asperity produces a "folding" mode of abrasion on ductile metals.[43] All this testifies again to the plasticity of an unreinforced PEG film. On the other hand, sharp-edged cracks are formed in NP-reinforced PEG films (Figure 4B), which indicates a somewhat more brittle behavior. This is consistent with the previous observations concerning the embrittlement caused by the NPs; however, in this case, cracks did not turn into delamination thanks to the stronger interface to the oxidized substrate. Notably, Jiang et al.[41] reported rather straight cracks across brittle polymers (e.g., unreinforced epoxy resins), whilst the cracks seen in the NPs-reinforced composites (Figure 4B) exhibit an irregular morphology, which likely results in crack deflection due to the NPs themselves. Hence, the NPs shift the coating's response from ductile to brittle, but at the same time exert some toughening action in this rather brittle material.

Because the surfaces of all samples are not perfectly smooth, it is somewhat difficult to pinpoint the exact load at which tears and cracks appear during the scratch test. However, an SEM inspection allows the estimation of critical loads for the onset of crack formation (which could be designated as L_{C1} according to the classification scheme proposed in the ISO 20502 standard, although that applies to ceramic films on metal substrates) as 9.75 ± 0.66, 7.47 ± 0.33, 6.49 ± 0.83, and 6.11 ± 0.65 N for the neat coating and the 5%, 10%, and 20% NPs composite coatings, respectively. This would confirm that the NPs reduce the film strength, albeit not very significantly when this strongly adheres to an oxidized titanium substrate.

The observed improved adhesion of the composite coating on the oxidized titanium substrate can be attributed to the formation of covalent bonds at the polymer/metal interface. As previously reported silane-terminated polymers can be easily covalently grafted to an oxidized metal surface[13] according to the scheme reported in **Figure 5**A. In the FT-IR spectra reported in Figure 5B, the arising band in the range of 3600–3000 cm^{-1} indicates that after 30 s treatment with a suitable oxidizing solution (H_2SO_4/H_2O_2, more detail in the Experimental Section), a significant formation of surface hydroxyl groups (—OHs) takes place.[44,45] Therefore, it is reasonable to assume that the OHs deriving from the oxidation of the titanium surface and OHs of silane-terminated polymer can condense by water elimination reaction, leading to the formation of covalent bonds at the interface, as previously described for similar systems.[46]

It has been demonstrated by Prasanna and Vijayaraghavan[19] that ZnO particles can catalyze the formation of ROSs when they are dispersed in an aqueous medium, not only under UV irradiation, but also in dark conditions. This is an important aspect since it opens the possibility to use ZnO particles also for applications where the sample cannot be irradiated by UV light, as in the case of coating of titanium implants. For this reason, the prepared nanocomposite coatings have been tested against *S. aureus* and *P. aeruginosa*, which are the Gram+ and Gram- strains that typically cause implant infections.[47,48] ATCC and clinical
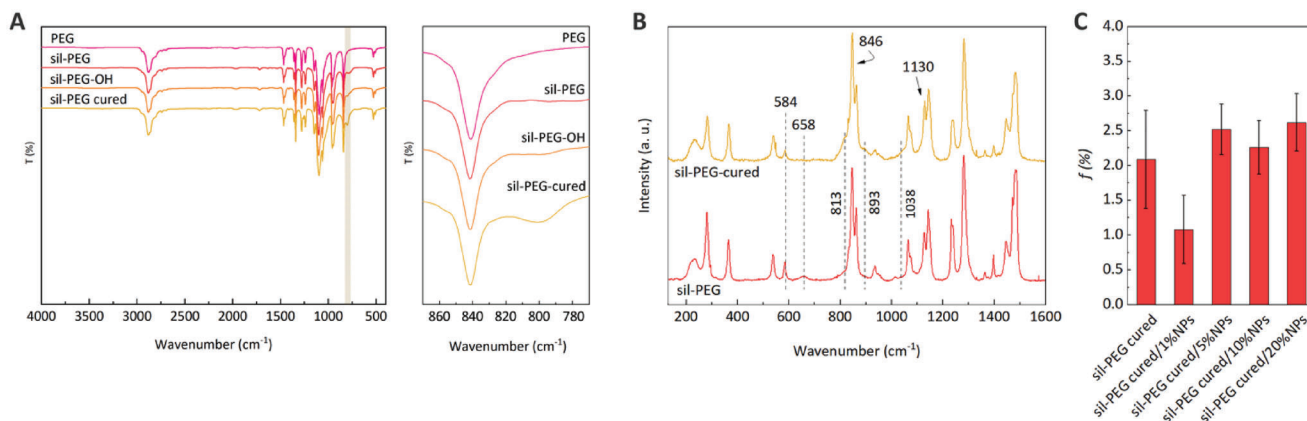

Figure 2. A) FT-IR spectra of PEG, sil-PEG, sil-PEG-OH, and sil-PEG cured. The inset reports the magnification in the range of 870–770 cm^{-1}. B) μRAMAN spectra of uncured and cured sil-PEG. C) Extractable fractions (*f*, calculated by Equation 2) of the neat and ZnO NPs-loaded sil-PEG after thermal curing.

**ADVANCED
SCIENCE NEWS**

www.advancedsciencenews.com

**ADVANCED
MATERIALS
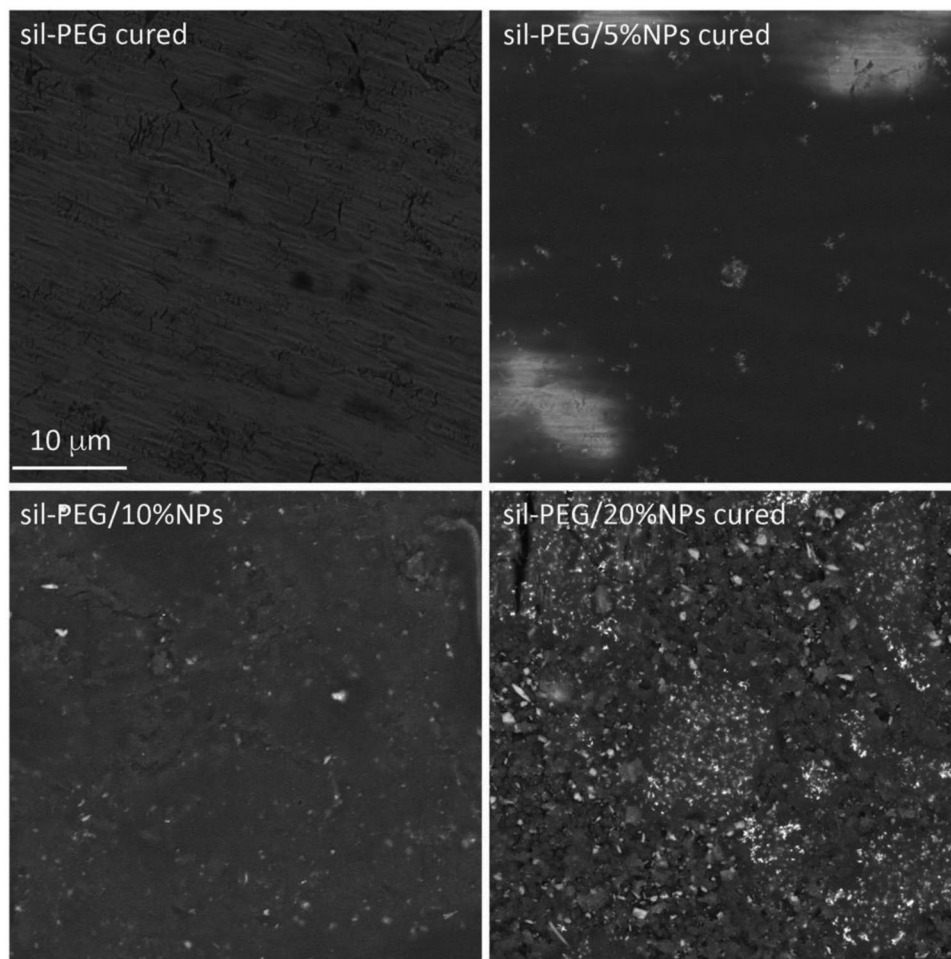INTERFACES**
Open Access

www.advmatinterfaces.de

Figure 3. Top-view FESEM images (back-scattered electrons) of the neat cured sil-PEG and nanocomposite coatings filled with 5, 10, and 20 wt% ZnO nanoparticles (NPs), respectively (scale bar is the same for all images).

strains of both bacteria have been tested. Especially for clinical strains, it is very important to have a very fast antibacterial effect to block the contamination of the implant and to inhibit the possible further development of an infection. Whether no contamination takes place during the surgical procedure, the consequent development of infection becomes less and less likely within the healing process. The time-kill curves (**Figure 6**A–C) show that by increasing the content of ZnO NPs the antibacterial activity against *S. aureus* is overall improved, whereas bare titanium and neat sil-PEG did not show a reduction in the viable cells. In particular, viable *S. aureus* ATCC 6538 cells decrease in contact with the composite coating after 8 h of incubation. A bactericidal activity is observed for the sil-PEG cured/20%NPs sample, which leads to the absence of viable *S. aureus* ATCC 6538 cells after 16 h of contact ($p = 0.01$, Figure 6A). Interestingly, the same trend is also found for the methicillin-resistant *S. aureus* P2 strain, as reported in Figure 6B. Similarly, the sil-PEG cured/20% NPs sample shows the best activity against the methicillin-resistant *S. aureus* P3 strain, where no viable cells are detected after 16 h ($p = 0.0007$, Figure 6C). sil-PEG cured/5% NPs and sil-PEG cured/10% NPs samples showed their antibacterial activity at the end of the experiment ($p < 0.05$) (Figure 6C).

Concerning *P. aeruginosa* ATCC 9027, high antibacterial activity is seen for the sil-PEG cured/20% NPs sample after 4 h of incubation, and no viable cells are found in the samples after 24 h. (Figure 6D). The samples containing 5 and 10% of NPs also showed remarkable antibacterial activity ($p = 0.008$ and 0.00109, respectively). As shown in Figure 6D, at the end of the experiment (24 h), samples 5% NPs and 10% NPs displayed significant differences compared with the negative controls (bare titanium substrate and neat sil-PEG $p = 0.0004$ and $p = 0.0002$, respectively).

Regarding the clinical strains of *P. aeruginosa* (Figure 6E,F) the samples that contain ZnO NPs show an acceptable antibacterial activity throughout the experiment, taking into account that clinical strains are in general more resistant than ATCC strains. As observed for *P. aeruginosa* ATCC 9027 strain, after 24 h the sil-PEG cured/20% NPs sample displayed the highest activity against *P. aeruginosa* 21 compared with the controls (Figure 6F).

In general, the coatings composed of 5 and 10 wt% NPs show a bacteriostatic activity and not bactericidal as for 20 wt%. However, these results are anyway remarkable considering that the initial bacterial contaminations used in the experiment are significantly
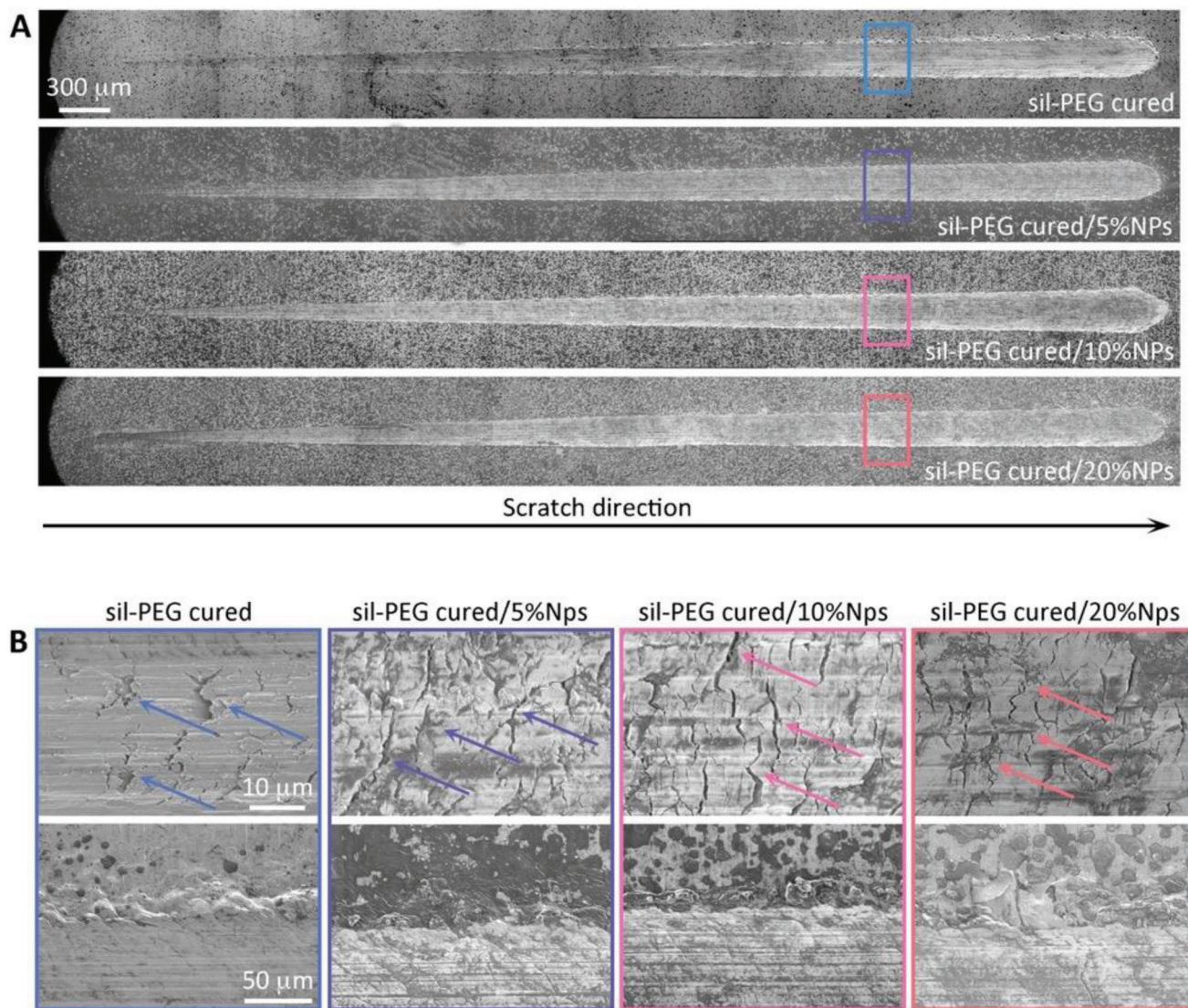
**ADVANCED
SCIENCE NEWS**

www.advancedsciencenews.com

**ADVANCED
MATERIALS
INTERFACES**

www.advmatinterfaces.de

Figure 4. Results of scratch tests performed on neat and ZnO NPs-modified sil-PEG coatings: A) overviews (optical microscopy) of the scratch tracks (all images have the same scale bar); B) SEM micrographs showing magnified views of the areas marked in Figure 4A. The upper figures show the magnification of the scratch tracks, while the lower figures show the edge of the scratch tracks (the images on the same row have all the same scale bars).

higher than what can be commonly found in an operating room. This ensures a much more promising antimicrobial activity in the actual application of the proposed coatings.

To corroborate the results of the time-kill tests (Figure 6), the viability of *S. aureus* ATCC 6538 and *P. aeruginosa* ATCC 9027 in contact with neat sil-PEG and coated samples (sil-PEG cured/5% NPs and sil-PEG cured/20% NPs) were analyzed using the fluorescence method. The method is based on the use of two nucleic acid dyes: propidium iodide (PI), a red fluorescent dye that penetrates only damaged cell membranes, and 5(6)-carboxyfluorescein diacetate (CFDA), a green fluorescent dye that penetrates all cell membranes (representative images are reported in Figure S3, Supporting Information).

As expected, the fluorescence assay shows that both *S. aureus* ATCC 6538 (**Figure 7**A) and *P. aeruginosa* ATCC 9027 (Figure 7B)

present an exponential growth, for 24 h of incubation, when they are not in contact with the antibacterial composite coating. On the other hand, when the bacteria are in contact with sil-PEG cured/5%NPs and sil-PEG cured/20%NPs, a significant decrease in the bacteria viability of both tested strains, over time, can be observed as shown by Figure 7C–F. Specifically, for these two composite coatings, very few viable cells are found already after 18 h of incubation if compared to the control experiments (Figure 7A,B) (p = 0.001 and p = 0.0003 for *S. aureus* and *P. aeruginosa*, respectively). After 24 h almost only dead cells can be detected (Figure 7C–F), with a significant reduction of viable bacteria compared to the control for both sil-PEG cured/5% NPs (p = 0.0006 and p = 0.0007 for *S. aureus* and *P. aeruginosa*, respectively) and sil-PEG cured/20% NP (p = 0.0007 and p = 0.0003 for *S. aureus* and *P. aeruginosa*, respectively).
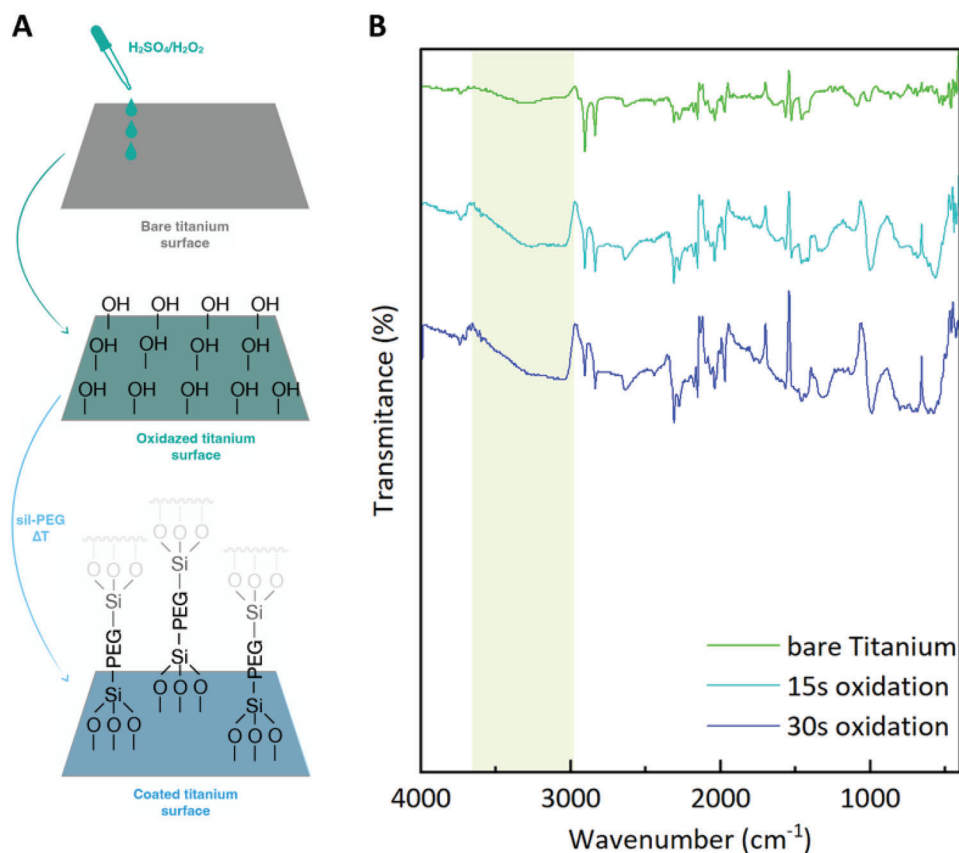
**ADVANCED
SCIENCE NEWS**

www.advancedsciencenews.com

**ADVANCED
MATERIALS
INTERFACES**
Open Access

www.advmatinterfaces.de

Figure 5. A) Schematic representation of the oxidation treatment and the consequent formation of hydroxyl groups (—OHs) and polymer grafting on the titanium surface. B) FT-IR spectra of the bare titanium and the oxidized surface after the treatment with the oxidizing solution for 15 and 30 s, respectively. Light green highlighted area shows the wide band associated with the formation of the OH groups on the titanium surface due to the oxidation treatment.

It has been reported that PEG-based substrates have a reduced bacterial biofilms adhesion.[49,50] Both *S. aureus* and *P. aeruginosa* bacterial strains have the ability to form biofilms, therefore we have also tested the anti-biofilm formation activity of the coating with 10% of NPs as a representative sample with an average content of the active material, at 4 and 24 h on ATCC and clinical strains of both bacteria (**Figure 8**). In general, after 4 h from the beginning of biofilm formation, only negligible differences have been observed for the tested bacterial strains on the different substrates. Mature biofilm formation (24 h) appears to be slightly lower on the coated sample with 10% NPs for both *S. aureus* strains (Figure 8A,B), probably due to the combined effect of PEG, which reduces the adhesion, and ZnO NPs as an antibacterial agent. On the other hand, for the two *P. aeruginosa* strains, lower anti-biofilm activity is not as clear as in the case of *S. aureus* strains observed in the first stage (4h) of biofilm formation (Figure 8C,D). In fact, for *P. aeuriginosa* 21, even greater biofilm growth has been observed in the presence of neat PEG (p = 0.0043) compared to bare titanium (Figure 8D). At 24h (mature biofilm), a small decrease of the biofilm formation is observed on the 10%NPs-coated samples, for both *P. aeruginosa* strains (p = 0.005) (Figure 8C,D). This is further confirmed by the investigations carried out by optical microscope that have shown slight eradication of biofilm structures and a small decrease in the number of adherent cells on coated samples compared to the two negative controls (bare titanium and neat sil-PEG substrates; Figure S4, Supporting Information).

Our results revealed a high efficiency of sil-PEG-cured surfaces/NPs against planktonic bacteria and limited activity in biofilm reduction. For the bacterial colonization of a surface to form a biofilm, the growth and migration of planktonic bacteria is essential. Therefore, antibacterial activity against planktonic bacteria is crucial for early containment of bacterial colonization. Biofilm is a structured community of microorganisms, enclosed in a self-produced polymeric matrix, adhering to an inert or living surface surrounded by an aqueous medium. Within the biofilm, there are multiple interactions between the different microbial species, which allow them to continuously adapt to extreme conditions and protect from external agents (e.g., disinfectants and antimicrobials). This complex structure is difficult to break down in the mature phase, but also in the initial phase of colonization and production of the biofilm, which causes an irreversible attachment to the surfaces. This explains the reason in our study the anti-biofilm activity is not remarkable, toward both the mature biofilm and after 4 h from the beginning of its formation on the tested substrates. Until now, studies on the anti-biofilm activity of functionalized ZnO NP surfaces have not shown always consistent results. More in detail, Applerot et al.[51] reported
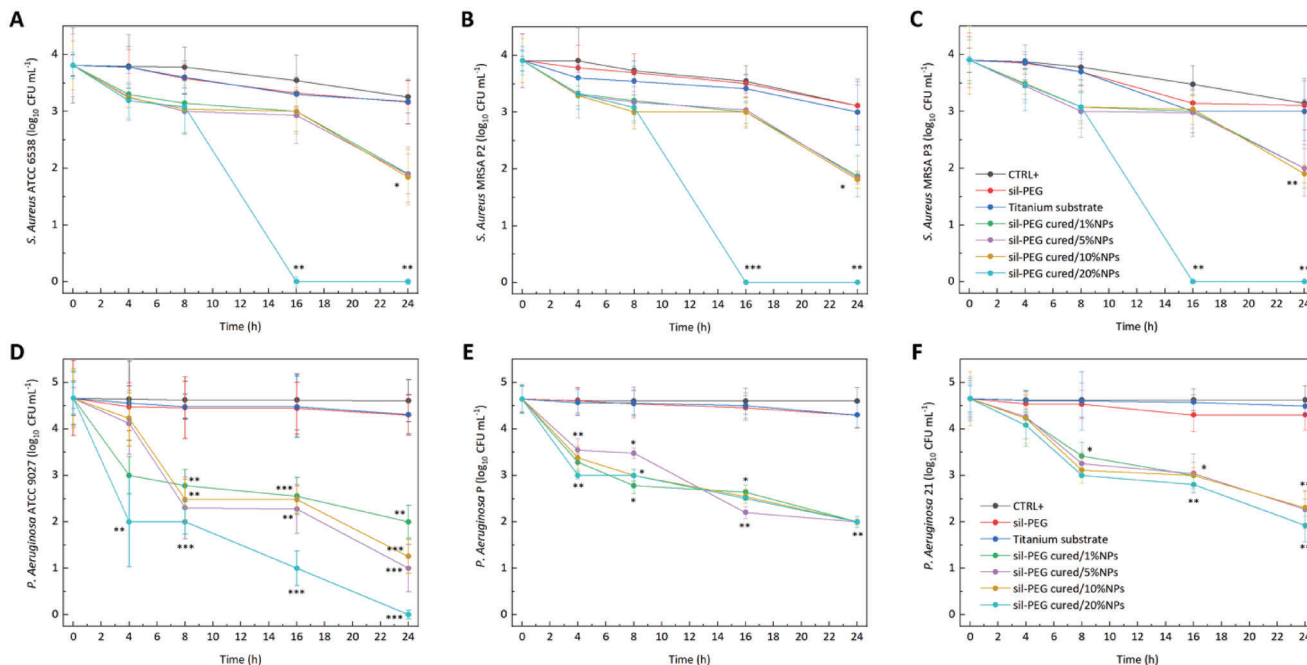
Figure 6. Time-kill curves of composite coatings and related negative controls (bare titanium substrate and neat sil-PEG) in contact with all tested bacterial strains: A) *S. aureus* ATCC 6538; B) *S. aureus* MRSA P2; C) *S. aureus* MRSA P3; D) *P. aeruginosa* ATCC 9027 E) *P. aeruginosa* P, and F) *P. aeruginosa* 21. CTRL+ is a suspension of tested bacteria not in contact with coatings. $p < 0.05$ (*), $p < 0.01$ (**), $p < 0.001$ (***), and $p < 0.0001$ (****) are considered significant by t-test and ANOVA with Bonferroni correction. Results were expressed as mean ± SD of the three determinations (error bar = S.D.; $n = 3$).
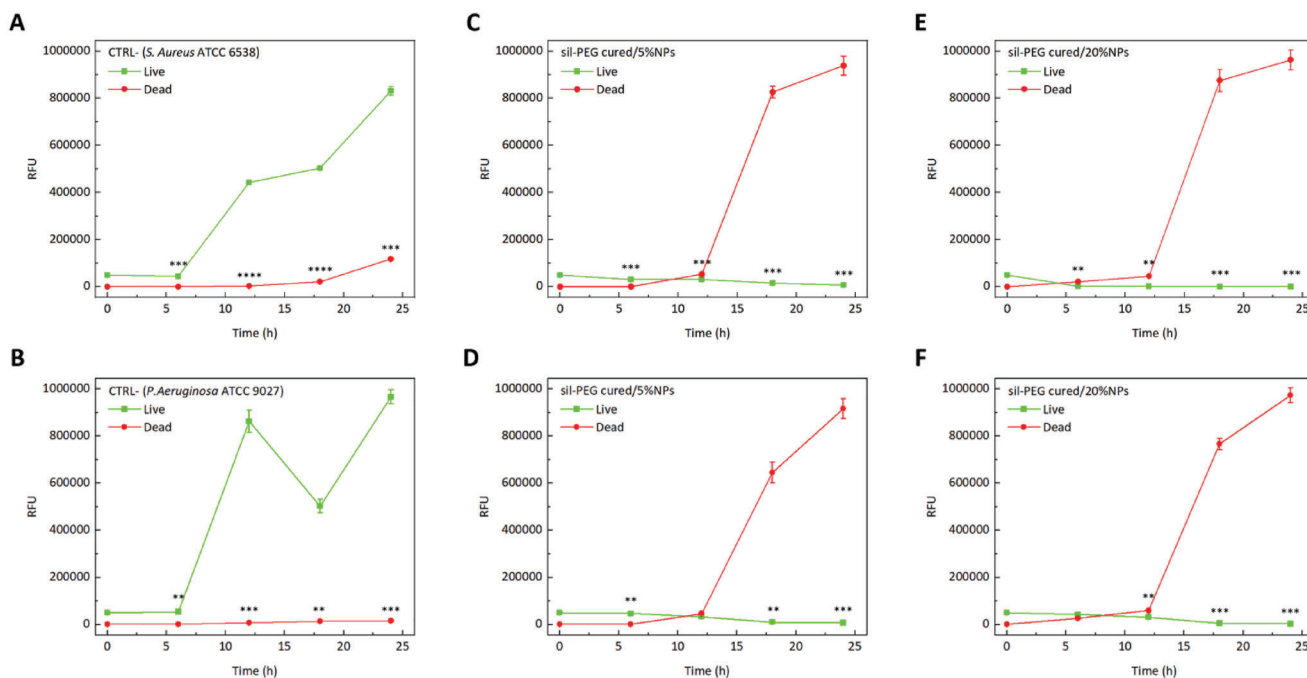

Figure 7. Bacterial growth kinetics and related live/dead cells quantification. Mean value of relative fluorescence units (RFU) of live and dead cells of A) *S. aureus* ATCC 6538 and B) *P. aeruginosa* ATCC 9027 in contact with neat sil-PEG coated sample as negative controls (CRTL-) for the tests. The same bacterial strains were also tested in contact with (C and D) sil-PEG cured/5%NPs and (E and F) sil-PEG cured/20%NPs coatings. Statistically significant differences between live and dead cells, $p < 0.05$ (*), $p < 0.01$ (**), $p < 0.001$ (***), and $p < 0.0001$ (****) are detected by t-test and ANOVA with Bonferroni correction. Results were expressed as mean ± SD of the three determinations (error bar = S.D.; $n = 3$).

**ADVANCED
SCIENCE NEWS**

www.advancedsciencenews.com

**ADVANCED
MATERIALS
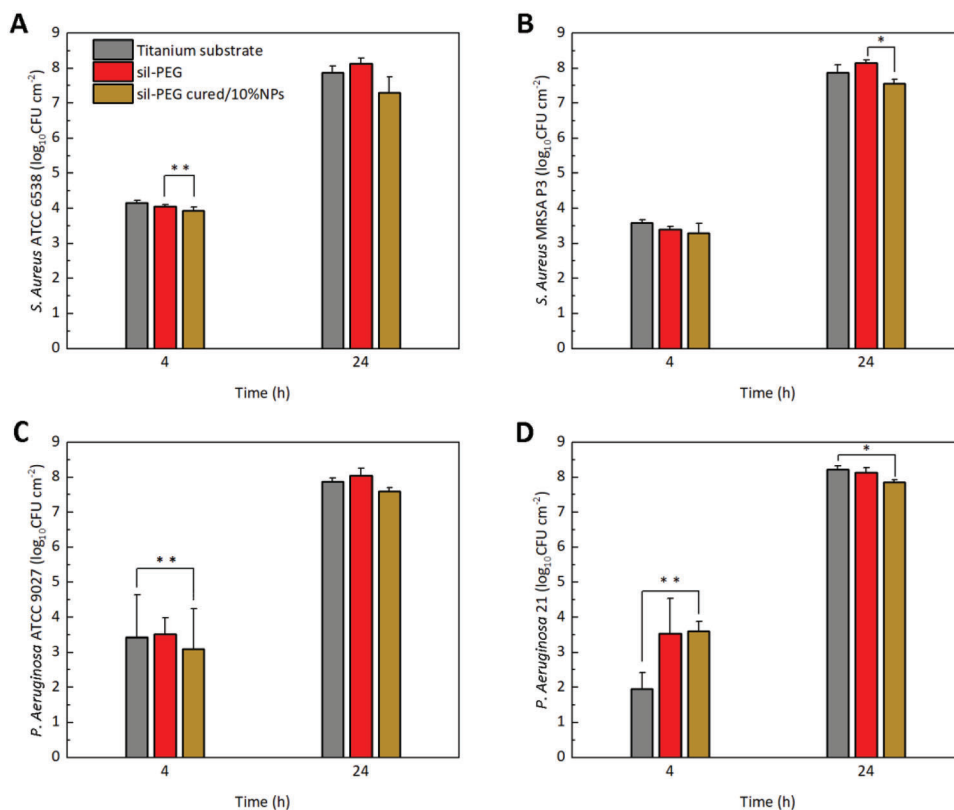INTERFACES**

www.advmatinterfaces.de

Figure 8. Anti-biofilm activity of sil-PEG cured/10%NPs against A) *S. aureus* ATCC 6538, B) clinical *S. aureus* MRSA P3, C) *P. aeruginosa* ATCC 9027, and D) clinical *P. aeruginosa* 21. Bare titanium substrate and neat sil-PEG samples are used as negative controls. $p < 0.05$ (*), $p < 0.01$ (**), $p < 0.001$ (***), and $p < 0.0001$ (****) are considered significant by *t*-test and ANOVA with Bonferroni correction. Results were expressed as mean ± SD of the three determinations (error bar = S.D.; $n = 3$).

an antibiofilm activity for a ZnO NP-derived coating with no decrease in cell viability. While other studies[52,53] displayed that NP-derived ZnO coatings allowed the formation of bacterial biofilms, but with less viable cells.

3. Conclusion

Sprayable formulations composed of silanized-PEG and ZnO nanoparticles have been herein proposed as an antibacterial coating for reducing post-surgery microbial infections of titanium implants. The silanization process of the PEG's terminals has been studied and successfully achieved. The sprayable thermosetting nanocomposite formulations, with increasing content of ZnO, have been optimized in order to obtain the desired coating adhesion, a homogeneous coverage, and no significant alterations of the metallic substrate aspect. In particular, the oxidation treatment of titanium substrates before the coating deposition significantly improved the adhesion of the composite coating that is intended for being applied onto metallic surfaces not subjected to cyclic movements and constant abrasion, but associated with low wear. Although the ZnO is embedded into the polymeric layer, the nanocomposite coatings show a significant antimicrobial activity, against *S. aureus* both ATCC and clinical strains, with nanoparticles content of 5 wt% within 24 h. The antimicrobial activity increases significantly when the nanoparticles content is increased to 20 wt%, resulting in coatings with

bactericidal properties within 16 h. Very similar results have been observed for ATCC strains of *P. aeruginosa*. On the other hand, when *P. aeruginosa* clinical strains have been used, bacteriostatic activity is observed due to the higher aggressive behavior of these strains that are also antibiotic-resistant. Knowing that even the partial growth inhibition of *P. aeruginosa* clinical strains has to be considered an appreciable result. The presented thermoset formulations can be used not only as antibacterial material for different applications, but also open up a new route to prepare sprayable active coatings in which changing the active nanoparticles or hydroxyl-terminated polymers a large variety of applications can be envisioned.

4. Experimental Section

Materials: Polyethylene glycol (PEG, average M_W 8000 g mol⁻¹), 3-isocyanatopropyltriethoxysilane (ICPTES), nitric acid (HNO₃) at 65% concentration, tetrahydrofuran (THF), ethanol (EtOH), acetone and zinc oxide (ZnO) NPs (<100 nm) were all supplied by Sigma–Aldrich and used as received without further purification. Titanium substrates (15 mm × 15 mm and 140 μm thick) were also purchased from Sigma–Aldrich and were used after cleaning the surface with 30 min sonication in acetone. After drying, titanium substrates were immersed for 30 s in a solution of an equal volume of sulfuric acid (H₂SO₄, ACS reagent, 95.0–98.0%, Sigma–Aldrich) and hydrogen peroxide (H₂O₂, 30% wt/wt, Sigma–Aldrich) in order to form an oxidized surface layer and thus improve the adhesion of the

**ADVANCED
SCIENCE NEWS**

www.advancedsciencenews.com

**ADVANCED
MATERIALS
INTERFACES**

www.advmatinterfaces.de

polymeric coating.[54] The titanium substrates were then further washed with distilled water and carefully dried before the spray-coating process.

PEG Terminals Modification: The silanization of PEG was carried out by a free-solvent approach following the reaction, as reported in Scheme 2. In detail, a given amount of PEG has been placed in a round-bottom flask and heated up to 120 °C by an oil bath. The system was kept under vigorous mechanical stirring and connected to nitrogen flow to obtain an inert environment. Once the polymer was completely melted, the ICPTES was added in a slight excess (ICPTES:PEG molar ratio of 2.2). The reaction was left running for 2 h, monitoring its evolution by FT-IR at different time intervals. At the end of the reaction, the obtained mixture was placed in a vacuum for a few minutes in order to remove, by evaporation, the possible unreacted ICPTES. Afterward, the silanized PEG (sil-PEG) was collected and stored in a fridge.

In order to obtain a low-temperature-curable oligomer, the ethoxy terminals of sil-PEG need to be substituted with hydroxyl groups (sil-PEG-OH, Scheme 3). Specifically, a solution of sil-PEG in THF (0.3 g mL^{-1}) was placed in a round-bottom flask and a solution containing EtOH, deionized water, and concentrated HNO$_3$ (weight ratio 26.6 g:9.8 g:2.9 g) was added (0.04 g of solution per 1 g of sil-PEG). The mixture was heated up to 60 °C and left stirring for 2 h. The resulting solution was further diluted with THF to achieve a sil-PEG-OH concentration of 0.03 g mL^{-1}. The desired amount of ZnO NPs was then added to the diluted sil-PEG-OH/THF solution and sonicated for 40 min by a water-bath sonicator. Besides the neat sil-PEG used for comparison reasons, four compositions with different ZnO NPs content were prepared: sil-PEG cured/1%NPs, sil-PEG cured/5%NPs, sil-PEG cured/10%NPs, and sil-PEG cured/20%NPs.

Coating Preparation: The as-prepared suspensions (1.5 mL per substrate) were sprayed on titanium substrates (15 × 15 mm^2) using a Timbertech ABPST01 air brusher (0.3 mm nozzle, siphon feed) positioned at 150 mm from the substrate and applying an air pressure of 2.5 bar. The spray-coated Ti substrates were placed in an oven at 65 °C for 24 h to activate the curing process (Scheme 1). In Figure S1 (Supporting Information), photographs of the produced coated substrates are reported.

Characterization: The silanization reaction and the titanium surface oxidation were followed by Fourier Transform Infrared (FT-IR) spectroscopy. For this purpose, a PerkinElmer Spectrum two spectrometer equipped with a diamond crystal was used in Attenuated Total Reflectance (ATR) mode, accumulating 32 scans with a resolution of 4 cm^{-1}. The reaction mixture (silanization) was sampled at different time points for 120 min (T_0 is just after the addition of ICPTES). Spectral data were processed with Spectrum 10 software (PerkinElmer).

The conversion (X) of the ICPTES was calculated by Equation 1 from the maximum intensity of the signal at 2270 cm^{-1}, which is associated with the stretching of the isocyanate group. The intensity of such a signal was normalized with respect to the constant signal at 1090 cm^{-1}, which corresponds to the stretching of the C—O—C bond.[55]

$$X\ (\%) = [1 - (I_t/I_0)] \cdot 100 \tag{1}$$

where I_0 and I_t are the normalized intensities of the isocyanate group signal (at 2270 cm^{-1}) at T_0 and different time points, respectively.

The uncured and cured sil-PEG were also analyzed by μRaman spectroscopy (Horiba Jobin-Yvon LabRAM HR800 μRaman Spectrometer). The μRaman spectrometer was equipped with a microscope and a 632.8 nm excitation line, in backscattering geometry through a 100× objective lens, was used to excite the specimens, at low power of 0.25 mW. The grating was 600 lines per mm with a spectral resolution of ≈ 1 cm^{-1}.

The fraction that does not form a covalently bonded polymeric network (extractable fraction, f) was evaluated on bulky specimens with the same composition of sprayed coatings. Specifically, the sil-PEG/THF suspensions were cast in molds and left to dry overnight. The obtained specimens were then cured a 65 °C for 24 h in the oven. The extraction tests were performed on ≈ 200 mg of each sample wrapped in a filter paper and immersed in 10 mL of THF for 24 h under gentle stirring, at room temperature. Afterward, the samples were removed from THF and dried at 60 °C under a dynamic vacuum up to constant mass. The extractable fraction of

each sample was normalized to the extractable fraction of the wrapping filter paper. The f values were calculated by the following equation:

$$f = [(m_0 - m_e)/m_0] \cdot 100 \tag{2}$$

where m_0 and m_e are the mass of the sample before and after the extraction test, respectively.

Field Emission gun Scanning Electron Microscopy (FESEM, Mira3, Tescan) was used to investigate the NPs distribution and for analyzing the thickness of the coating. The coated Ti substrates were attached on a stub by carbon tab and analyzed by applying an accelerating voltage of 5 kV. The samples were previously coated by electro-deposition method with ≈ 10 nm of gold.

Scratch tests (Micro-Combi Tester, Anton Paar Tritec, Corcelles, CH) were performed using a Rockwell C-type conical diamond indenter (120° aperture) with a rounded tip (200 μm radius). Tests were performed in "progressive loading" mode according to the ISO 20502 standard, i.e., the load was increased linearly along the scratch track, from 0.02 to 30 N along a 6 mm-long track, advancing at a speed of 1 mm min^{-1}. The critical loads for the onset of failure were identified by inspecting the scratch tracks both with an optical microscope (200× magnification) and a Scanning electron microscope (Nova NanoSEM 450, FEI Thermo Fisher Scientific, Eindhoven, NL). Three tests were performed on each sample.

Antibacterial Activity: *Bacterial Strains*: Both reference (ATCC-American Type Culture Collection) and clinically isolated bacterial strains were used. Gram-positive *Staphylococcus aureus* ATCC 6538, two strains of methicillin-resistant *Staphylococcus aureus* (MRSA), *Pseudomonas aeruginosa* ATCC 9027, and two clinical *Pseudomonas aeruginosa* were grown in Tryptic Soy Broth (TSB, Oxoid, Italy) supplemented with 0.6% yeast extract (TSB-YE, Oxoid, Italy) and kept at 37 °C for 24 h. All cultures were centrifuged at 2000 rpm for 20 min. After discarding the supernatant fluid, the pellets were re-suspended in 5 mL of deionized water. Centrifugation, supernatant discard, and re-suspension were repeated three times. The obtained suspensions were stored until use in phosphate-buffered saline supplemented with 30% (vol/vol) glycerin at −80 °C.

Time-Kill Experiment: For the antibacterial quantitative evaluation, coated samples (15 × 15 mm^2) were added in 10 mL saline solution (NaCl 0.85%) suspensions of all the test strains (10^4 CFU mL^{-1}). The suspensions were incubated at 37 °C for 24 h with an oscillating speed of 150 rpm, and bacterial counts were determined, at regular intervals, by spreading serial tenfold dilutions on selective agar plates (Mannitol Salt Agar for *S. aureus* and MacConkey Agar for *P. aeruginosa*, Oxoid, Italy). Neat sil-PEG and titanium substrates were tested as negative controls. A suspension of each test strain not in contact with the coated sample was used as a bacterial growth control (positive control). The experiments were replicated three times.

Bacterial Growth Kinetics: Growth kinetics were evaluated for *S. aureus* ATCC 6538 and *P. aeruginosa* ATCC 9027, using the fluorescence method. Coated samples (sil-PEG cured/5% NPs and sil-PEG cured/20% NPs) were placed in contact with overnight cultures of the tested bacteria (≈ 10^4 CFU mL^{-1}), in sterile phosphate-buffered saline solution (PBS), and stained by the "live/dead cells stain kit" (Thermo Fisher Scientific, USA) according to manufacturer instructions. The method is based on the use of propidium iodide (PI) as a marker of dead cells and 5(6)-carboxyfluorescein diacetate (CFDA) to detect live cells. All samples were incubated at 37 °C under agitation inside a multi-well plate fluorescence reader (Synergy HTX, BIOTEK, USA). Every 6 h, the number of viable and dead cells of indicator strains placed in contact with the coated samples, was compared by fluorescence readings to that of a control suspension in contact with a neat sil-PEG coated sample (CRTL-). The results are expressed in fluorescence units (RFU). The "live/dead cells stain kit" method is based on using propidium iodide (PI) to mark dead cells (PI excitation/emission: 528/645 nm) and 5(6)-CFDA to determine viable cells (CFDA excitation/emission: 485/528 nm). Following the 24 h experiments, 100 μL aliquots of each sample were taken and placed on a slide for analysis under a fluorescence microscope (Normaski DIC optics. Nikon Instruments Inc., USA).

Biofilm Tests: The mature biofilm produced by all the strains was obtained by introducing the coated samples (sil-PEG cured/10% NPs) in 12-well polystyrene microtiter plates, containing Tryptic Soy Broth (TSB, Oxoid, Italy) added with $\approx 10^4$ CFU mL^{-1} of single microbial strains and incubated at 37 °C for 4 and 24 h. After biofilm formation, the samples were washed three times with sterile PBS solution (pH 7.2) to remove unattached cells, sonicated for 15 min, and vortexed. Serial tenfold dilutions of the obtained re-suspensions were spread onto selective agar plates for the viable cell count (CFU cm^{-2}). The colonies were counted following incubation at 37 °C for 24 h. Titanium-substrate and sil-PEG were also tested as negative controls.

The biofilm on the coated samples was washed three times with sterile PBS and the attached cells were fixed with paraformaldehyde for 1 h at 4 °C. Subsequently, the surfaces were washed twice with sterile PBS and 150 µL of crystal violet (CV) solution at 0.1% was added to stain both the cellular component and the biofilm matrix. After incubation for 30 min at room temperature, the unbound dye was removed by washing three times with sterile PBS and a sticky tape was glued from the adhesive side to the samples for 15 min at room temperature. Then, for better visualizing the biofilm, the tape with adherent CV-stained biofilms was removed and placed on a glass microscope slide.[56] The slides were analyzed by a Light Microscope Nikon Eclipse 90i imaging system equipped with Nomarski DIC optics (Nikon Instruments, Melville, NY, USA). DS-2Mv Nikon digital camera was employed to obtain images. Ti-substrate and sil-PEG were also tested as negative controls.

Statistical Analysis: The statistical significance was determined by the *t*-test and ANOVA test using the statistical program GraphPad Prism 9.2.0. (San Diego, CA, USA). The analysis was followed by Bonferroni's post hoc test. The *p*-values were declared significant at ≤ 0.05. Each experiment was replicated three times under the same conditions.

Supporting Information

Supporting Information is available from the Wiley Online Library or from the author.

Acknowledgements

Conflict of Interest

The authors declare no conflict of interest.

Author Contributions

D.M. (0000-0003-3231-7769) performed conceptualization, investigation, data curation, funding acquisition, supervision, visualization, wrote original draft, and reviewed and edited the manuscript. R.I. (0000-0003-3071-3258) performed investigation, data curation, wrote original draft, and reviewed and edited the manuscript. E.L.P. (0000-0001-5959-9730) performed investigation, data curation, and wrote original draft. G.B. (0000-0001-7894-9476) performed investigation, wrote original draft and resources. C.S. (0000-0003-3221-5172) collected resources. M.D.E. (0000-0002-4513-8527) performed investigation, supervision, and wrote original draft and reviewed and edited the manuscript. P.F. (0000-0002-1903-8290) performed conceptualization and funding acquisition

Data Availability Statement

The data that support the findings of this study are available from the corresponding author upon reasonable request.

Keywords

[1] G. W. Leeson, *J. Popul. Ageing* **2018**, *11*, 107.
[2] L. Partridge, J. Deelen, P. E. Slagboom, *Nature* **2018**, *561*, 45.
[3] M. Tieland, I. Trouwborst, B. C. Clark, *J. Cachexia Sarcopenia Muscle* **2018**, *9*, 3.
[4] S. Gautam, D. Bhatnagar, D. Bansal, H. Batra, N. Goyal, *Biomed. Eng. Adv.* **2022**, *3*, 100029.
[5] Y. Sato, N. Kitagawa, A. Isobe, *Japan. Dental Sci. Rev.* **2018**, *54*, 45.
[6] J. Mouhyi, D. M. Dohan Ehrenfest, T. Albrektsson, *Clin. Implant Dent. Relat. Res.* **2012**, *14*, 170.
[7] N. Broggini, L. M. McManus, J. S. Hermann, R. Medina, R. K. Schenk, D. Buser, D. L. Cochran, *J. Dent. Res.* **2006**, *85*, 473.
[8] S. Lischer, E. Körner, D. J. Balazs, D. Shen, P. Wick, K. Grieder, D. Haas, M. Heuberger, D. Hegemann, *J. R. Soc. Interface* **2011**, *8*, 1019.
[9] J. G. Bartlett, *N. Engl. J. Med.* **2004**, *350*, 1422.
[10] R. Wang, K. G. Neoh, Z. Shi, E.-T. Kang, P. A. Tambyah, E. Chiong, *Biotechnol. Bioeng.* **2012**, *109*, 336.
[11] M. E. Davey, G. A. O'toole, *Microbiol. Molecul. Biol. Rev.* **2000**, *64*, 847.
[12] C. Even, C. Marlière, J. M. Ghigo, J. M. Allain, A. Marcellan, E. Raspaud, *Adv. Colloid Interface Sci.* **2017**, *247*, 573.
[13] H. Chouirfa, H. Bouloussa, V. Migonney, C. Falentin-Daudré, *Acta Biomater.* **2019**, *83*, 37.
[14] Z. Y. Qiu, C. Chen, X. M. Wang, I. S. Lee, *Regen. Biomater.* **2014**, *1*, 67.
[15] H. Koivuluoto, *J. Therm. Spray Technol.* **2022**, *31*, 1750.
[16] M. Wang, D. Duday, E. Scolan, S. Perbal, M. Prato, C. Lasseur, M. Hołyńska, *Adv. Mater. Interfaces* **2021**, *8*, 1.
[17] S. M. Dizaj, F. Lotfipour, M. Barzegar-Jalali, M. H. Zarrintan, K. Adibkia, *Mater. Sci. Eng. C* **2014**, *44*, 278.
[18] Y. Li, W. Zhang, J. F. Niu, Y. S. Chen, *ACS Nano* **2012**, *6*, 5164.
[19] V. Lakshmi Prasanna, R. Vijayaraghavan, V. L. Prasanna, R. Vijayaraghavan, *Langmuir* **2015**, *31*, 9155.
[20] X. Xu, D. Chen, Z. Yi, M. Jiang, L. Wang, Z. Zhou, Y. Fan, Y. Wang, D. Hui, *Langmuir* **2013**, *29*, 5573.
[21] D. Morselli, P. Valentini, G. Perotto, A. Scarpellini, P. P. Pompa, A. Athanassiou, D. Fragouli, *Compos. Sci. Technol.* **2017**, *149*, 11.
[22] L. Shu-Cai, L. Ya-Na, *J. Appl. Polym. Sci.* **2010**, *116*, 2965.
[23] P. Molitor, V. Barron, T. Young, *Int. J. Adhes. Adhes.* **2001**, *21*, 129.
[24] M. Zhang, X. H. Li, Y. D. Gong, N. M. Zhao, X. F. Zhang, *Biomaterials* **2002**, *23*, 2641.
[25] B. D. Fairbanks, M. P. Schwartz, C. N. Bowman, K. S. Anseth, *Biomaterials* **2009**, *30*, 6702.
[26] M. Catauro, F. Bollino, F. Papale, M. Gallicchio, S. Pacifico, *Mater. Sci. Eng., C* **2015**, *48*, 548.
[27] C. M. Xing, F. N. Meng, M. Quan, K. Ding, Y. Dang, Y. K. Gong, *Acta Biomater.* **2017**, *59*, 129.
[28] M. Iotti, P. Fabbri, M. Messori, F. Pilati, P. Fava, *J. Polym. Environ.* **2009**, *17*, 10.
[29] P. Fabbri, C. Leonelli, M. Messori, F. Pilati, M. Toselli, P. Veronesi, S. Morlat-Thérias, A. Rivaton, J. L. Gardette, *J. Appl. Polym. Sci.* **2008**, *108*, 1426.
[30] R. Iseppi, S. De Niederhäusern, I. Anacarso, P. Messi, C. Sabia, F. Pilati, M. Toselli, M. D. Esposti, M. Bondi, *Soft Matter* **2011**, *7*, 8542.

[31] E. C. Tarakci, T. N. Gevrek, *Eur. Polym. J.* **2022**, *175*, 111338.

[32] M. Aghabararpour, M. Mohsenpour, S. Motahari, A. Abolghasemi, *J. Non Cryst. Solids* **2018**, *481*, 548.

[33] A. Fidalgo, L. M. Ilharco, *Chemistry* **2004**, *10*, 392.

[34] E. A. Sagitova, K. A. Prokhorov, G. Y. Nikolaeva, A. V. Baimova, P. P. Pashinin, A. Y. Yarysheva, D. I. Mendeleev, *J. Phys. Conf. Ser.* **2018**, *999*, 012002.

[35] U. Posset, M. Lankers, W. Kiefer, H. Steins, G. Schottner, *Appl. Spectrosc.* **1993**, *47*, 1600.

[36] M. Schmitt, *RSC Adv.* **2014**, *4*, 1907.

[37] D. Fischer, D. Pospiech, U. Scheler, R. Navarro, M. Messori, P. Fabbri, *Macromol. Symp.* **2008**, *265*, 134.

[38] A. A. Issa, A. S. Luyt, *Polymers* **2019**, *11*, 537.

[39] L. Black, in *Spectroscopic Properties of Inorganic and Organometallic Compounds.*, Vol. *40*, The Royal Society Of Chemistry, Cambridge **2009**, pp. 72–127.

[40] D. Siniscalco, M. Dutreilh-Colas, Z. Hjezi, J. Cornette, N. El Felss, E. Champion, C. Damia, *Ceramics* **2019**, *2*, 372.

[41] H. Jiang, R. Browning, H. J. Sue, *Polymer* **2009**, *50*, 4056.

[42] P. Kurkcu, L. Andena, A. Pavan, *Wear* **2014**, *317*, 277.

[43] A. Mahato, Y. Guo, N. K. Sundaram, S. Chandrasekar, *Proc. Royal Soc. A: Mathematical, Phys. Eng. Sci.* **2014**, *470*, 20140297.

[44] P. M. Kumar, S. Badrinarayanan, M. Sastry, *Thin Solid Films* **2000**, *358*, 122.

[45] R. Atchudan, T. N. Jebakumar Immanuel Edison, S. Perumal, D. Karthikeyan, Y. R. Lee, *J. Photochem. Photobiol. A Chem.* **2017**, *333*, 92.

[46] S. P. Pujari, L. Scheres, A. T. M. Marcelis, H. Zuilhof, *Angew. Chem. – Intl. Ed.* **2014**, *53*, 6322.

[47] P. Huang, K. Ma, X. Cai, D. Huang, X. Yang, J. Ran, F. Wang, T. Jiang, *Colloids Surf. B Biointerfaces* **2017**, *160*, 628.

[48] B. M. Geilich, T. J. Webster, *Int. J. Nanomed.* **2013**, *8*, 1177.

[49] K. W. Kolewe, J. Zhu, N. R. Mako, S. S. Nonnenmann, J. D. Schiffman, *ACS Appl. Mater. Interfaces* **2018**, *10*, 2275.

[50] K. Dong Park, Y. Soo Kim, D. Keun Han, Y. Ha Kim, E. Hee Bae Lee, H. Suh, K. Suk Choi, *Biomaterials* **1998**, *19*, 851.

[51] G. Applerot, J. Lellouche, N. Perkas, Y. Nitzan, A. Gedanken, E. Banin, *RSC Adv.* **2012**, *2*, 2314.

[52] T. Jansson, Z. J. Clare-Salzler, T. D. Zaveri, S. Mehta, N. V. Dolgova, B.-H. Chu, F. Ren, B. G. Keselowsky, *J. Nanosci. Nanotechnol.* **2012**, *12*, 7132.

[53] M. J. McGuffie, J. Hong, J. H. Bahng, E. Glynos, P. F. Green, N. A. Kotov, J. G. Younger, J. S. VanEpps, *Nanomedicine* **2016**, *12*, 33.

[54] A. Michiardi, G. Hélary, P. C. T. Nguyen, L. J. Gamble, F. Anagnostou, D. G. Castner, V. Migonney, *Acta Biomater.* **2010**, *6*, 667.

[55] K. Yuniarto, Y. A. Purwanto, S. Purwanto, B. A. Welt, H. K. Purwadaria, T. C. Sunarti, *AIP Conf. Proc.* **2016**, *1725*, 1.

[56] R. Iseppi, R. Feminò, C. Sabia, P. Messi, *Adv. Microbiol., Infect. Dis. Public Health* **2020**, *14*, 127.